Low-dimensional quantum magnetism in $Cu(NCS)_2$: A molecular framework material

Matthew J. Cliffe,[1] Jeongjae Lee,[1] Joseph A. M. Paddison,[2] Sam Schott,[2] Paromita Mukherjee,[2] Michael W. Gaultois,[1] Pascal Manuel,[3] Henning Sirringhaus,[2] Siân E. Dutton,[2] Clare P. Grey[1,*]

March 30, 2018

[1]Department of Chemistry, University of Cambridge,
Lensfield Road, Cambridge, CB2 1EW, U.K.
[2]Cavendish Laboratory, Department of Physics, University of Cambridge,
JJ Thomson Avenue, Cambridge CB3 0HE, United Kingdom
[3]ISIS Facility, STFC Rutherford Appleton Laboratory,
Harwell Oxford, Didcot OX11 0QX, United Kingdom *To whom correspondence should be addressed;
e-mail: cpg27@cam.ac.uk.

Contents

List of Figures

List of Tables

1 Linear-response determination of Hubbard U

As Hubbard-U parameters are sensitive to the local bonding environment around the transition metal atom,[S1] we therefore calculated linear-response U parameter for $Cu(NCS)_2$ using the method of Cococcioni *et al.*[S2] In brief, the U-parameter was obtained by the variation of d-orbital occupation, n, on application of a perturbing potential on the d-orbital, α. Two sets of calculations were performed, one where the initial, non-U charge was fixed (producing the non-selfconsistent gradient $\chi = dn/d\alpha$) and another where the charge was allowed to relax (producing the self-consistent gradient χ_0). From these two gradients, an approximate measure of U-parameter is obtained by $U = 1/\chi_0 - 1/\chi$ (ESI Fig. 1).

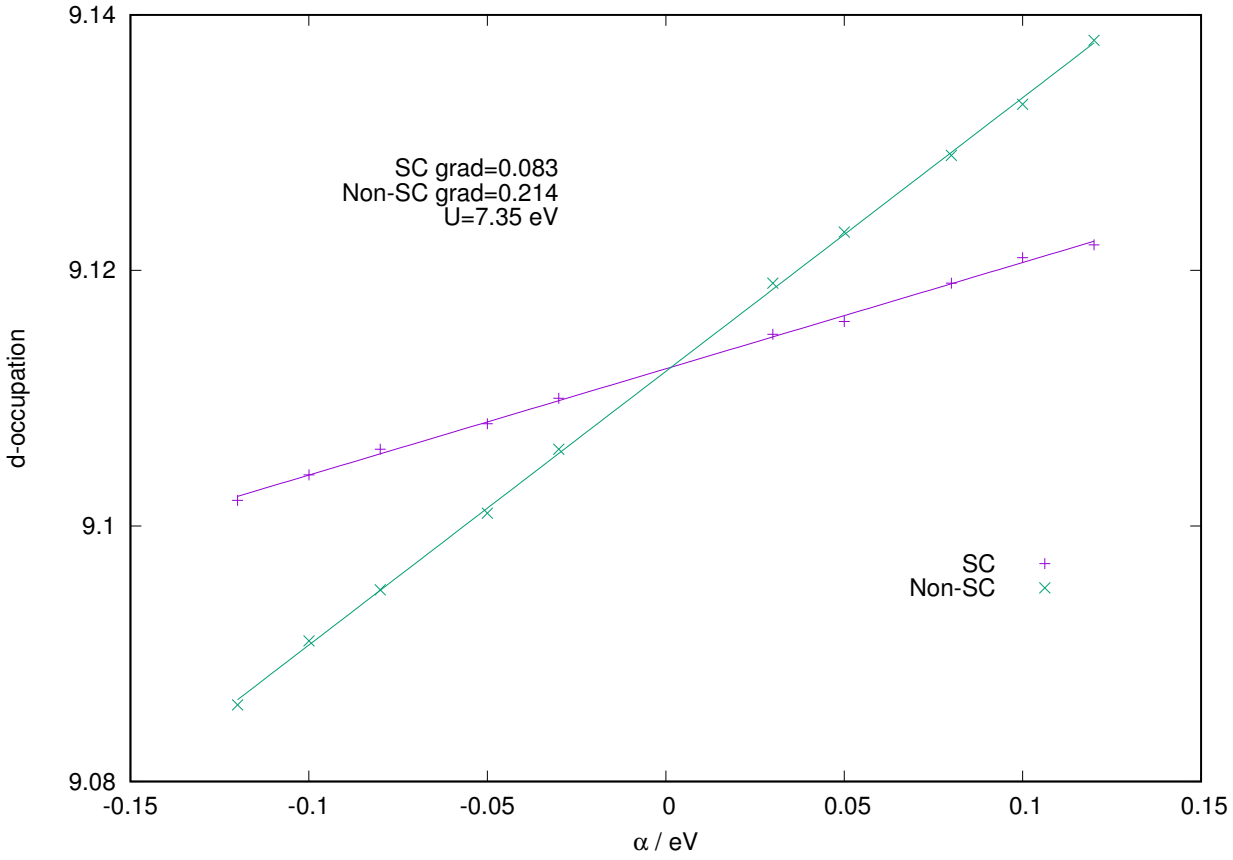

ESI Fig. 1: Determination of linear-response Hubbard-U of Cu^{2+} in $Cu(SCN)_2$.

2 Derivation of the NMR scaling parameter

In paramagnetic NMR, the effect of the electronic spin on the nuclear spin transition energies (i.e. the paramagnetic contribution to the overall shift) can be divided into the (Fermi) contact and pseudocontact shift. The pseudocontact shift, although permitted due to the anisotropy of the susceptibility tensor (only the $d_{x^2-y^2}$ orbital is half occupied), is expected to be much smaller than the dominant contact shift considered here as it obeys a $1/r^3$ dependency.[S3, S4] Similarly, zero-field splitting was not taken into account as it is anticipated to be small.

We will be making use of the following fundamental physical quantities:

Bohr radius (m)	$r_0 = 5.29177 \times 10^{-11}$
Avogadro constant (1/mol)	$N_A = 6.02214 \times 10^{23}$
^{13}C nuclear g-factor	$g_I = 1.40483$
Electron g-factor	$g_e = 2.00232$
Bohr magneton (J/T)	$\mu_B = 9.274 \times 10^{-24}$
Nuclear magneton (J/T)	$\mu_N = 5.051 \times 10^{-27}$
Vacuum permeability (N/A^2)	$\mu_0 = 4\pi/10^6$

The Fermi contact shift, $\delta_{\text{iso}}^{\text{FC}}$, under a static magnetic field, B_0, is defined as the ratio of nuclear spin transition energy and the nuclear Zeeman transition energy,

$$\delta_{\text{iso}}^{\text{FC}} = 10^6 \frac{\Delta E_{\text{hyperfine}}}{\Delta E_{\text{Zeeman}}}. \tag{1}$$

For the single-quantum NMR transition condition, the nuclear and electronic spin transitions have following selection rules: $\Delta m_I = \pm 1$, $\Delta m_S = 0$, and $m_S = \pm\frac{1}{2}$, giving

$$\delta_{\text{iso}}^{\text{FC}} = 10^6 \frac{A_{\text{iso}} m_S m_I}{B_0 g_I \mu_N m_I}, \tag{2}$$

where A_{iso} is the hyperfine coupling constant, defined as

$$A_{\text{iso}} = \frac{2}{3}\mu_0 \mu_B \mu_N g_e g_I \left|\psi^{\alpha-\beta}\right|^2 \tag{3}$$

where $\left|\psi^{\alpha-\beta}\right|^2$ is the spin density at the nucleus. This can be recast in terms of the Boltzmann-averaged molar susceptibility, χ_M, by making use of the small field approximation $B_0\chi_M = \mu_0\mu_B g_e N_A \langle S_z \rangle$,[S3] to give

$$\delta_{\text{iso}}^{\text{FC}} = 10^6 \frac{A_{\text{iso}}}{N_A \mu_0 g_e g_I \mu_N \mu_B} \chi_M. \tag{4}$$

By substituting in Eqn. 2, the following expression is obtained:

$$\delta_{\text{iso}}^{\text{FC}} = \underbrace{\frac{2}{3}\left(\frac{10^6 \left|\psi^{\alpha-\beta}\right|^2}{N_A r_0^3}\right)}_{\Phi} \chi_M \tag{5}$$

which allows us to define the prefactor Φ used in the main text.

3 Electron Paramagnetic Resonance Parameters

ESI Table 1: Fitted parameters for the variable temperature EPR measurements

T(K)	Gaussian line width (mT)	Lorentzian line width (mT)	g_{xx}	g_{yy}	g_{zz}
5	1.17104	8.94661	2.22928	2.05212	2.02711
6	1.12732	9.0893	2.22832	2.04341	2.02434
7	0.71548	9.49644	2.21909	2.5345	2.02361
8	0.61208	5.53544	2.2167	2.05615	2.0109
9	0.37446	5.56726	2.21647	2.05557	2.01078
10	0.50034	5.66748	2.21634	2.05482	2.01065
11	0.61531	5.70181	2.21632	2.05431	2.01042
12	0.63089	5.06405	2.21554	2.05507	2.00988
13	0.73589	5.31363	2.21806	2.05457	2.00879
14	0.52685	5.08888	2.21521	2.05511	2.01016
16	0.48592	5.66617	2.21496	2.05472	2.01106
30	0.27047	7.24215	2.2148	2.05398	2.01207
40	1.32577	11.70834	2.21558	2.04967	2.0183
50	1.32577	16.41945	2.21338	2.03252	2.03841
60	2.68047	20.25992	2.20817	2.03894	2.03844
70	1.32573	24.25718	2.19301	2.04474	2.0462
80	1.49525	26.97614	2.18333	2.04769	2.05236
100	1.45084	31.73852	2.18595	2.04762	2.0476
120	1.39839	35.47717	2.19056	2.04307	2.04724
160	1.32574	41.9804	2.19521	2.03853	2.04453
200	1.35114	47.06426	2.20063	2.04025	2.03831
240	1.32577	52.22019	2.19867	2.03519	2.03935
290	1.23988	55.85819	2.22261	2.02942	2.02933

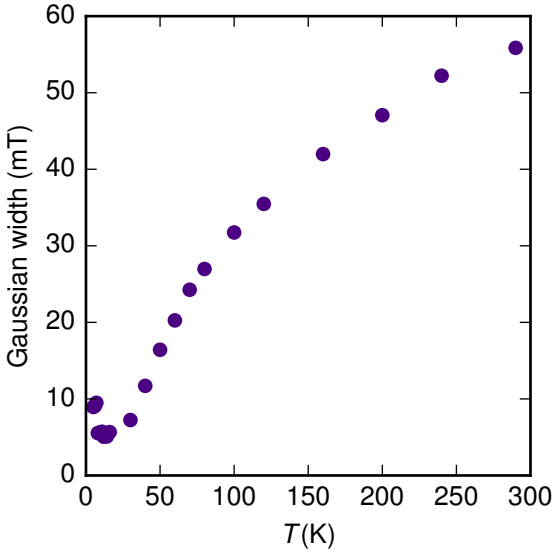

ESI Fig. 2: Temperature dependence of the EPR Gaussian line width

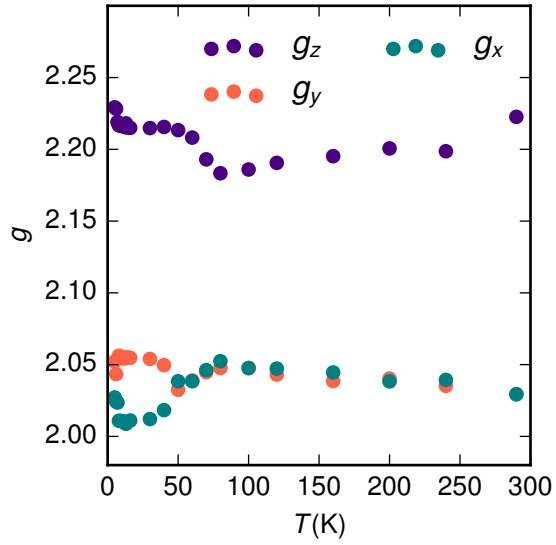

ESI Fig. 3: Temperature dependence of the g-factor determined from EPR

4 Powder Diffraction Refinements

ESI Table 2: Coefficients of thermal expansion along the principal axes

Axis	α (MK^{-1})	$\mathbf{X_n} \cdot \mathbf{a}$	$\mathbf{X_n} \cdot \mathbf{b}$	$\mathbf{X_n} \cdot \mathbf{c}$
X_1	$-12.9(1.7)$	0.63	0.75	0.19
X_2	$17.7(1.3)$	0.87	0.14	-0.48
X_3	$51.8(4.2)$	0.61	-0.49	0.63
V	$59(4)$			

Standard error given in brackets. The direction of the principal axes (normalized eigenvectors) given in fractional coordinates.

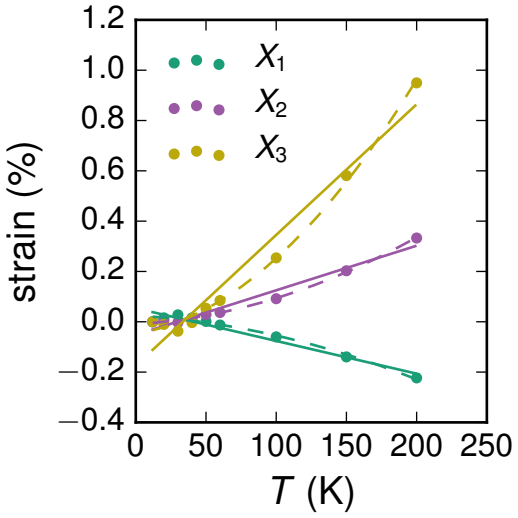

ESI Fig. 4: Principal axes of strain calculated from lattice parameters derived from Pawley refinement of laboratory X-ray diffraction data. Linear fit to data shown as solid line, quadratic fit illustrated by dashed line.

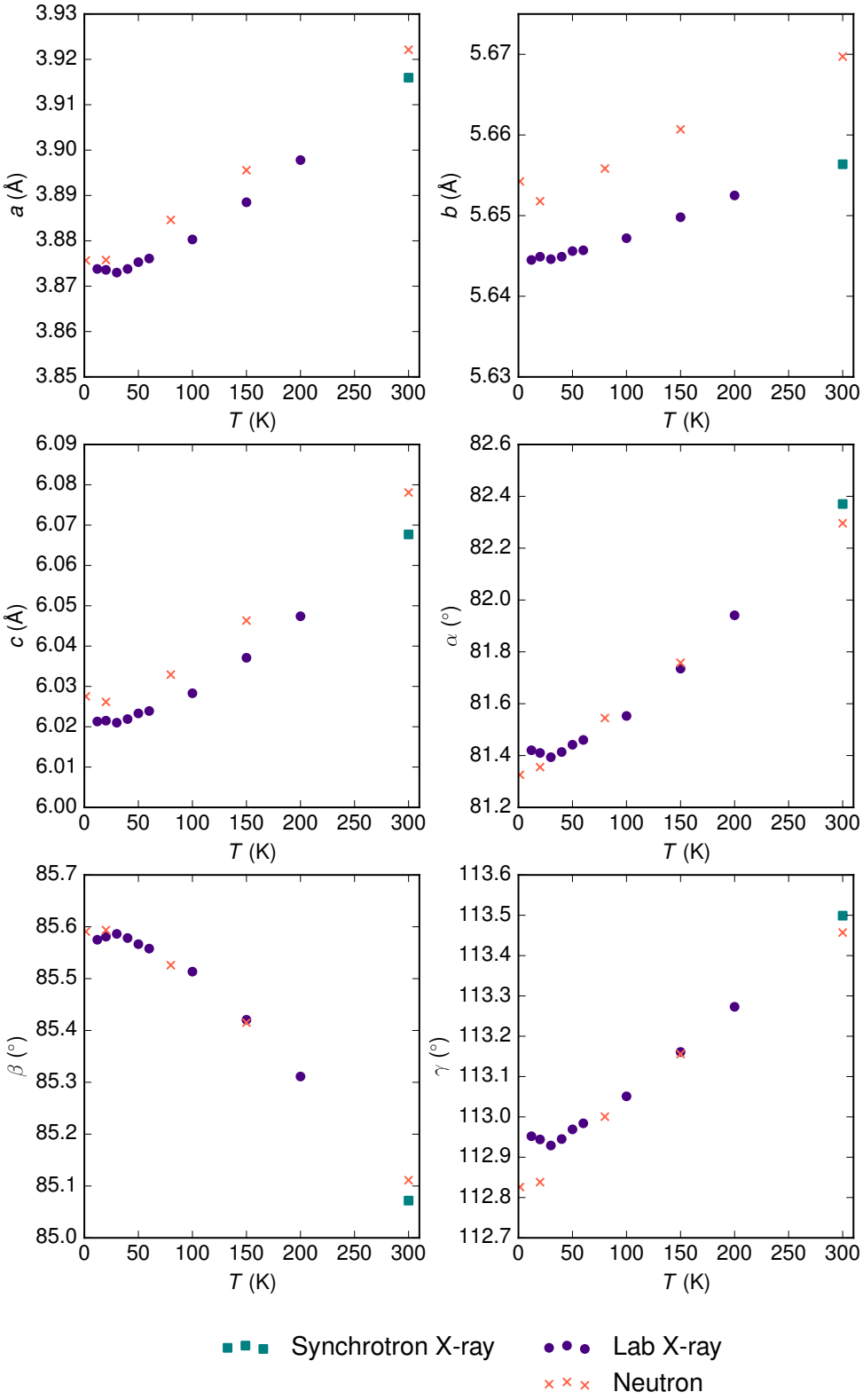

ESI Fig. 5: Variation in lattice parameters with temperature derived from Pawley (lab X-ray) or Rietveld (synchrotron and neutron) refinement diffraction data.

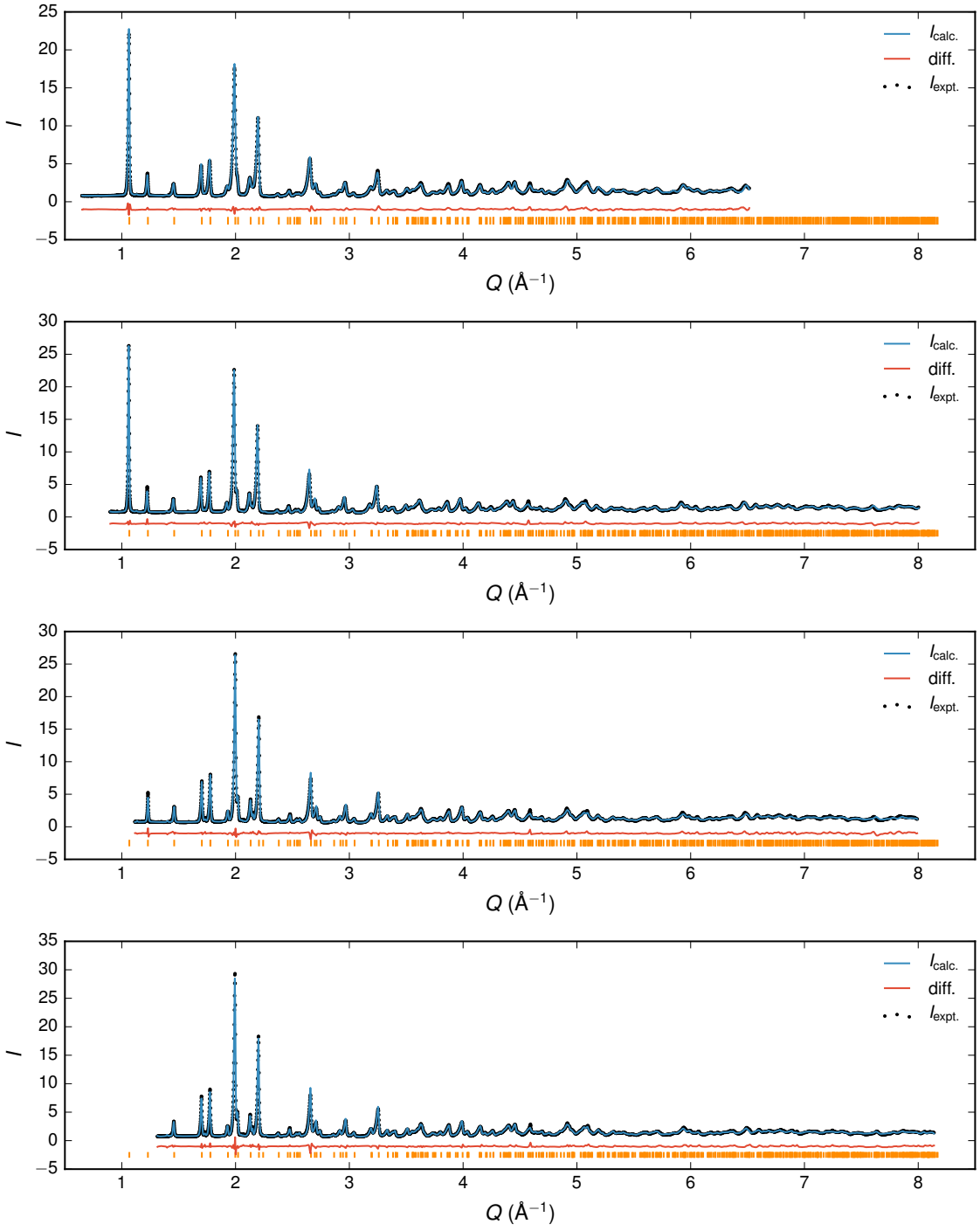

ESI Fig. 6: Neutron Rietveld Refinement at 1.4 K. From top to bottom, banks 2, 3, 4 and 5.

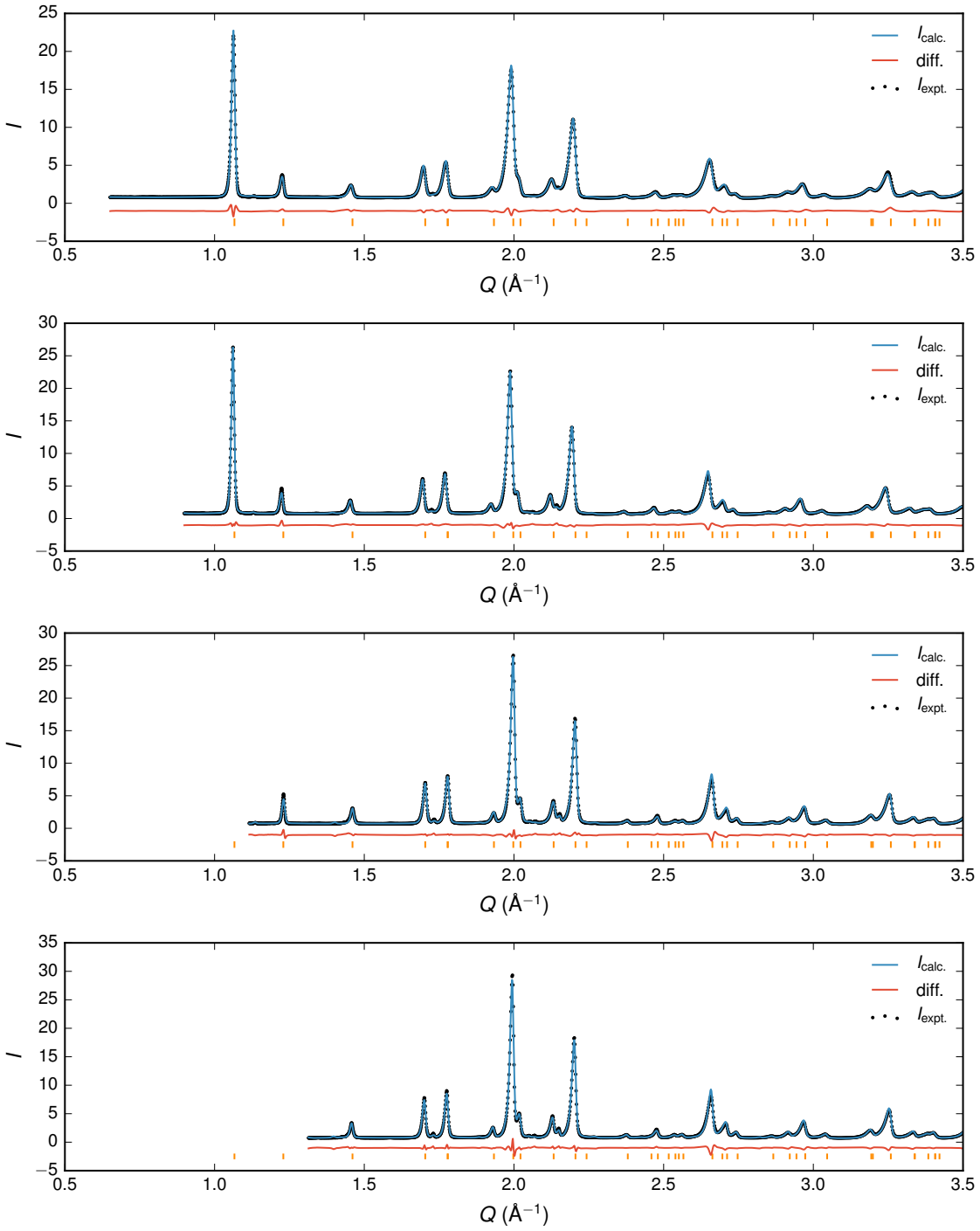

ESI Fig. 7: Neutron Rietveld Refinement at 1.4 K for the low Q region. From top to bottom, banks 2, 3, 4 and 5.

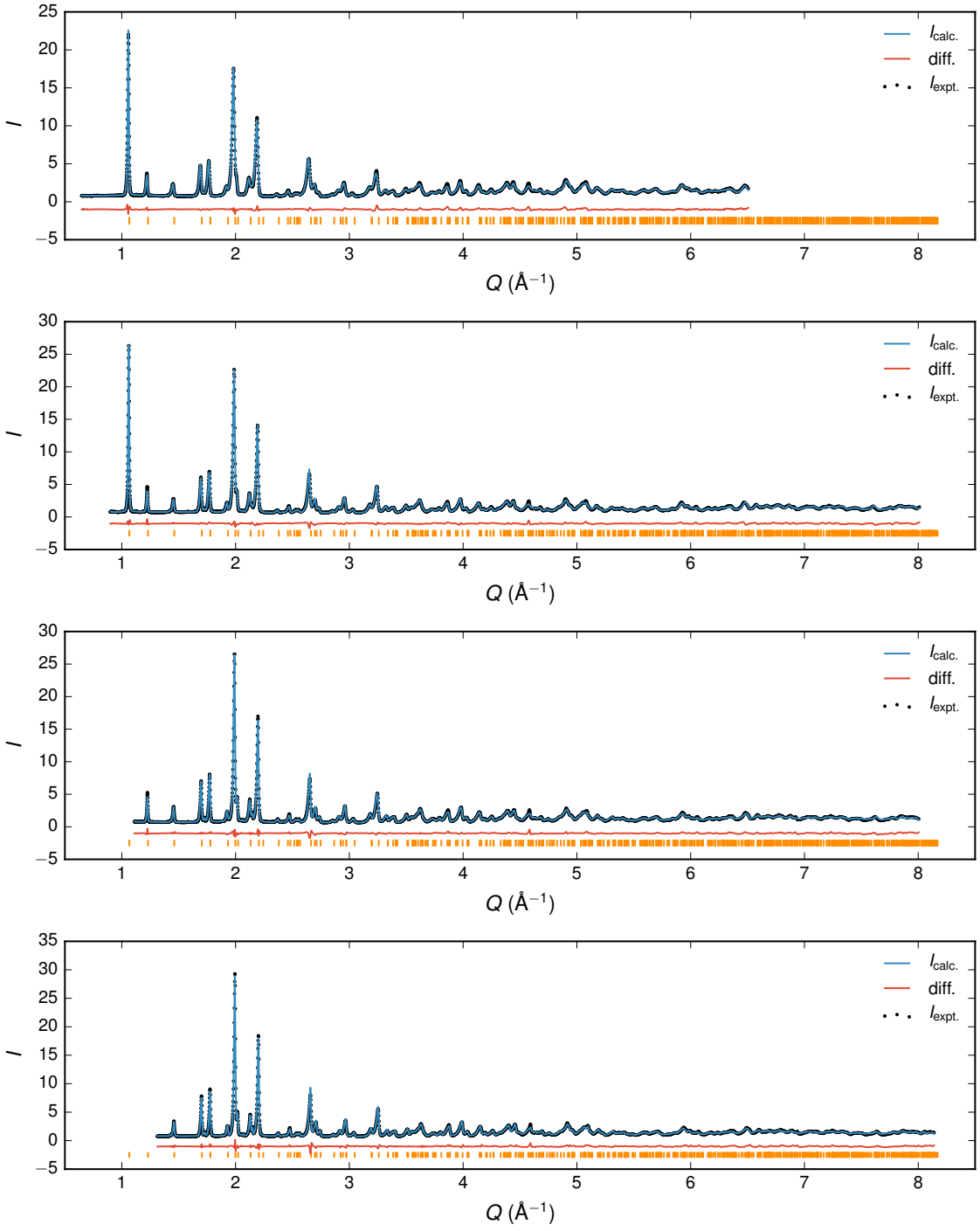

ESI Fig. 8: Neutron Rietveld Refinement at 20 K. From top to bottom, banks 2, 3, 4 and 5.

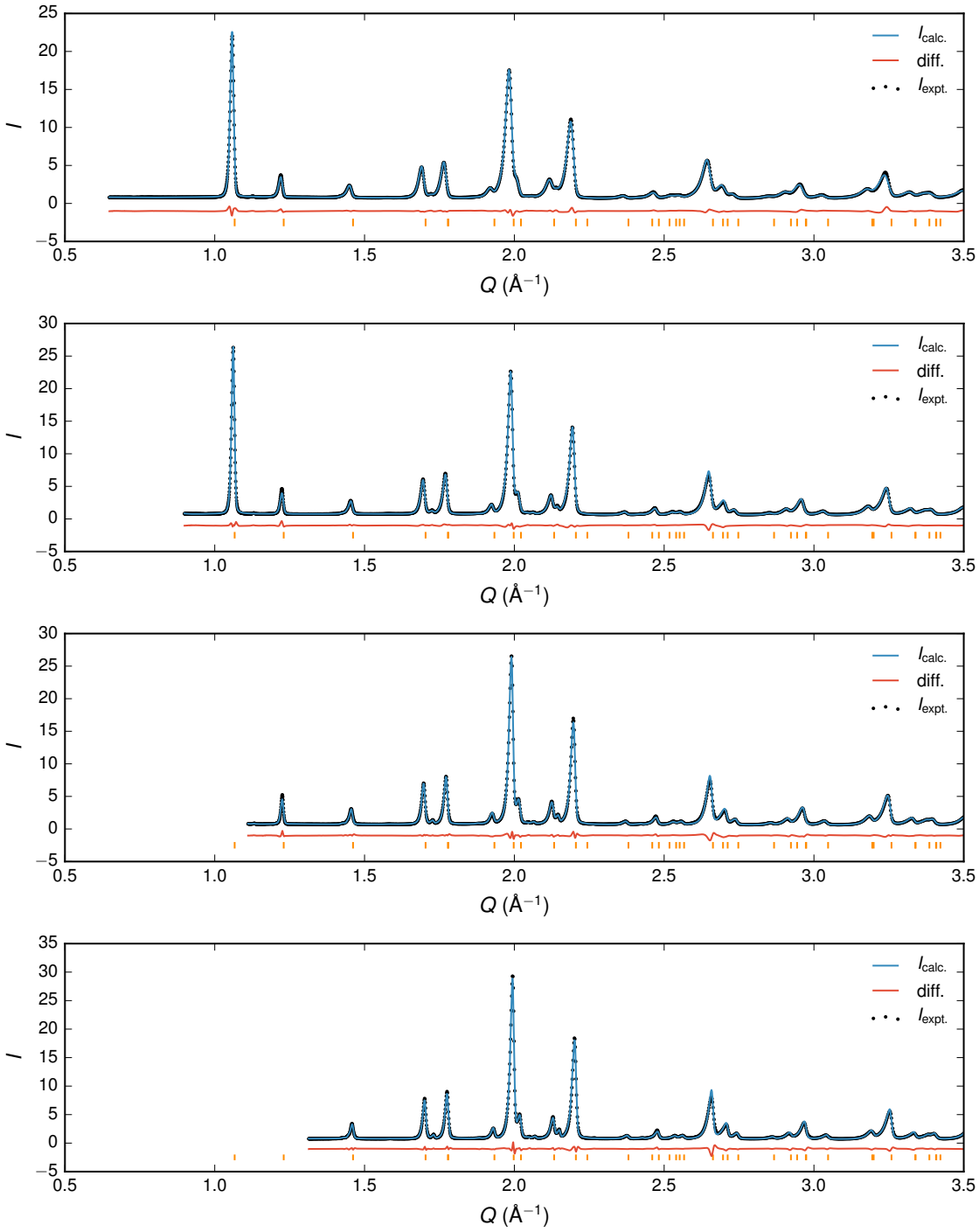

ESI Fig. 9: Neutron Rietveld Refinement at 20 K for the low Q region. From top to bottom, banks 2, 3, 4 and 5.

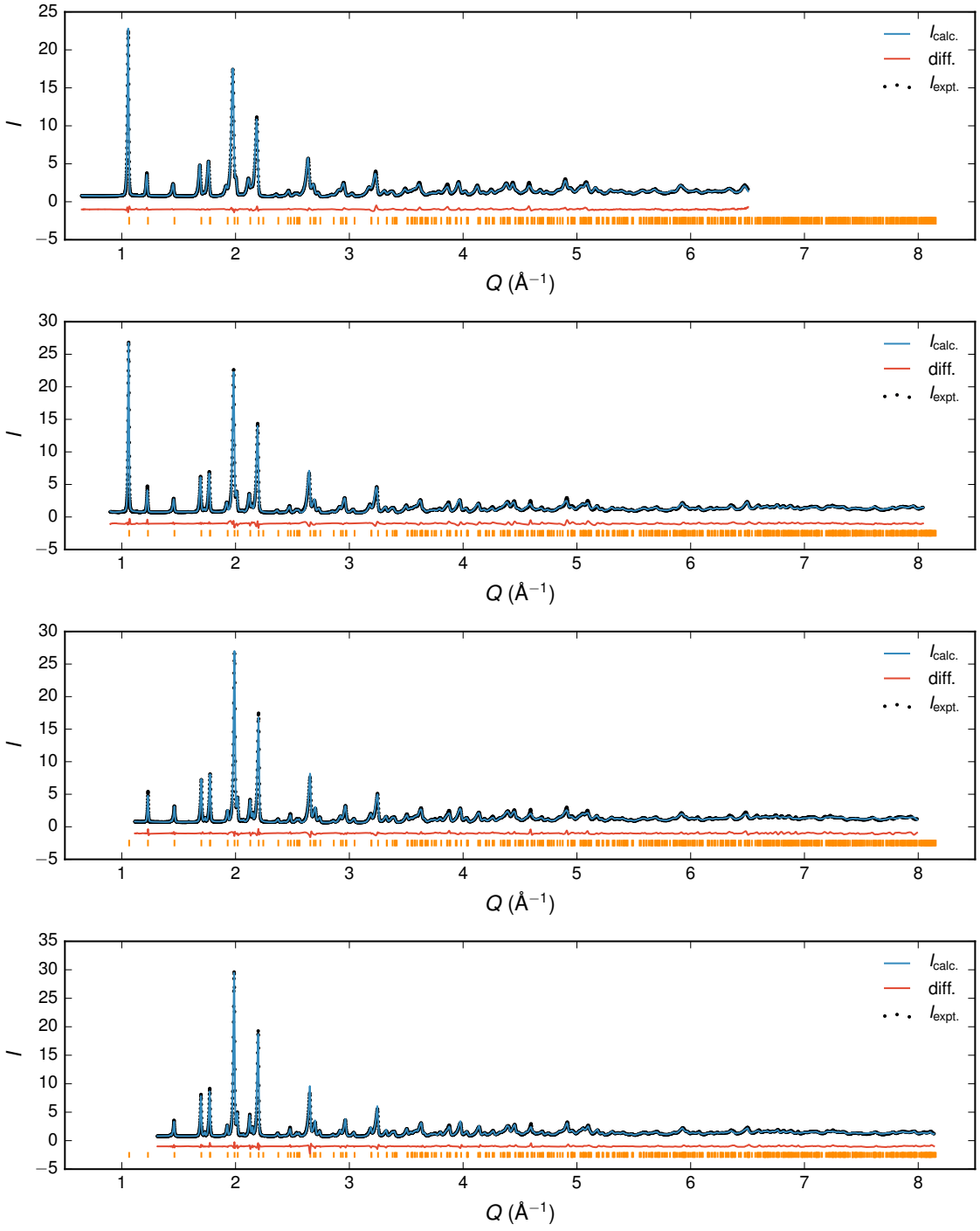

ESI Fig. 10: Neutron Rietveld Refinement at 80 K. From top to bottom, banks 2, 3, 4 and 5.

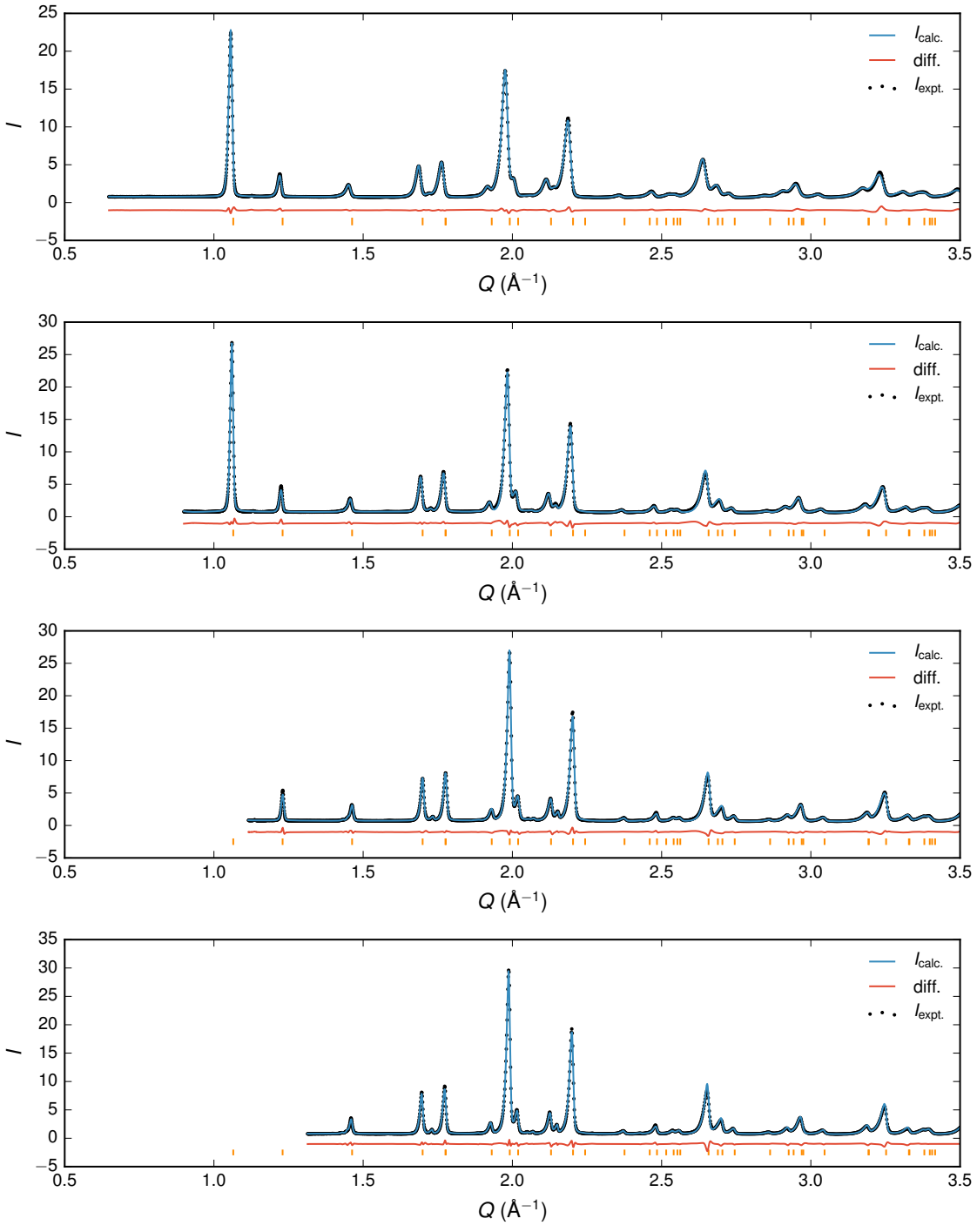

ESI Fig. 11: Neutron Rietveld Refinement at 80 K for the low Q region. From top to bottom, banks 2, 3, 4 and 5.

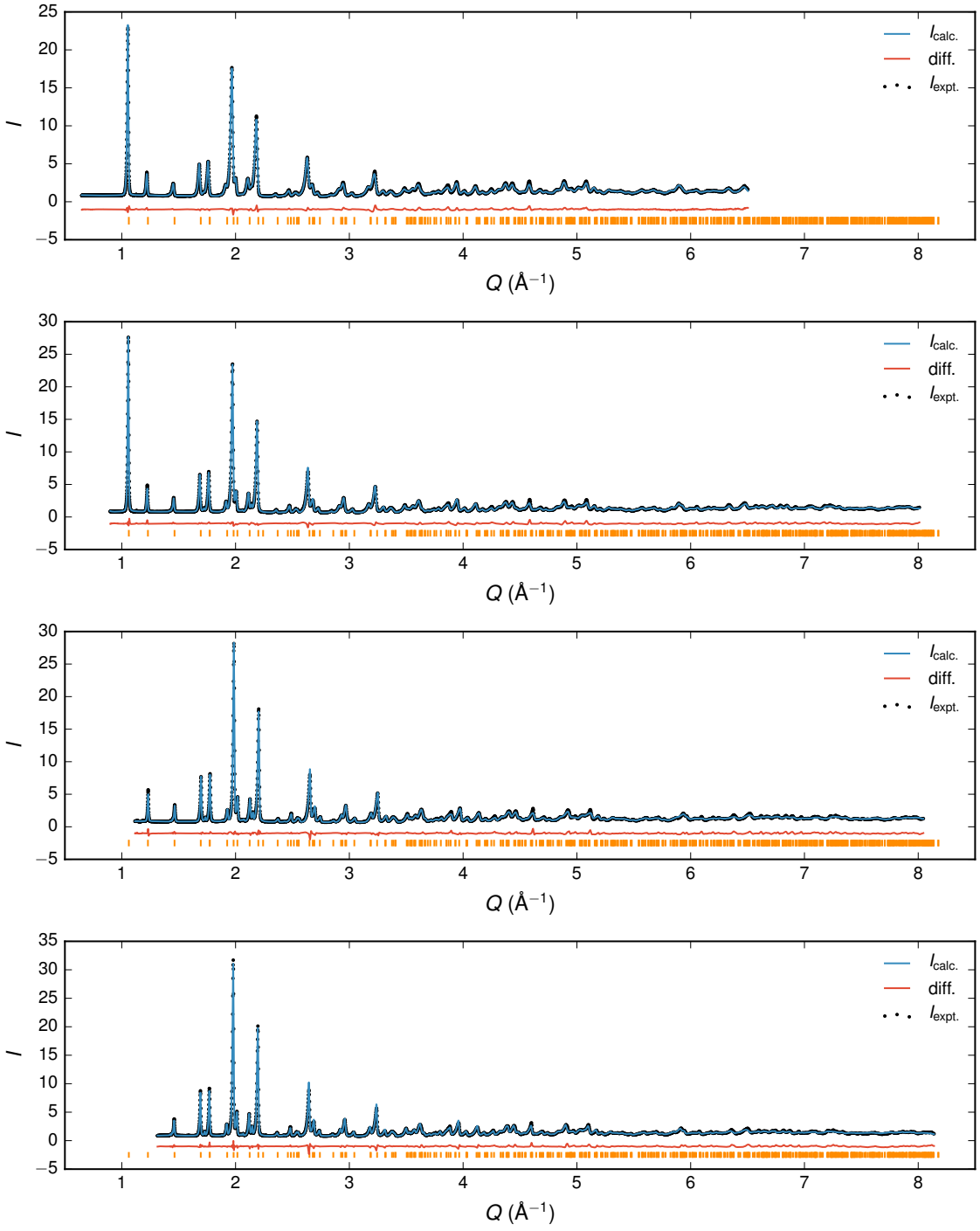

ESI Fig. 12: Neutron Rietveld Refinement at 150 K. From top to bottom, banks 2, 3, 4 and 5.

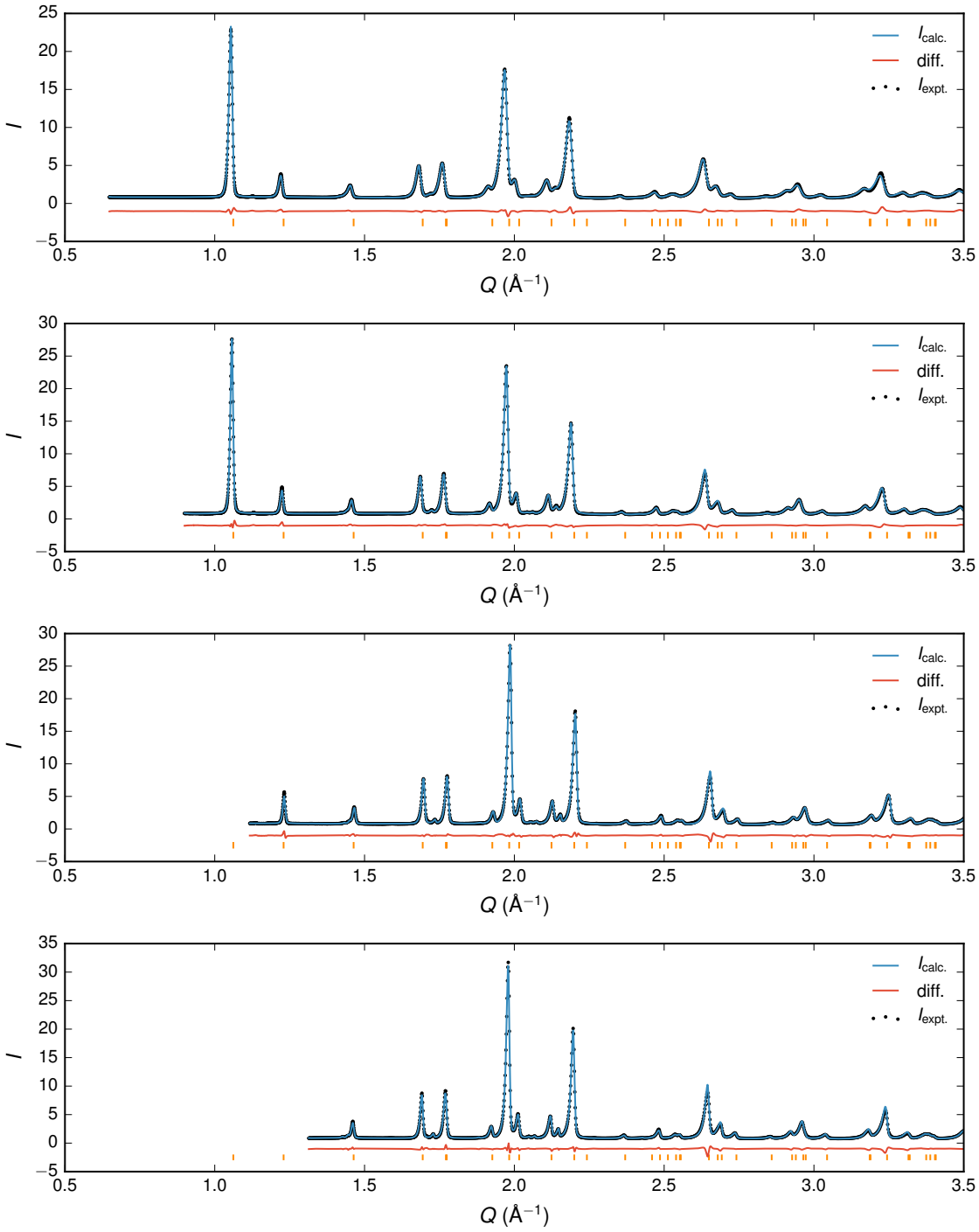

ESI Fig. 13: Neutron Rietveld Refinement at 150 K for the low Q region. From top to bottom, banks 2, 3, 4 and 5.

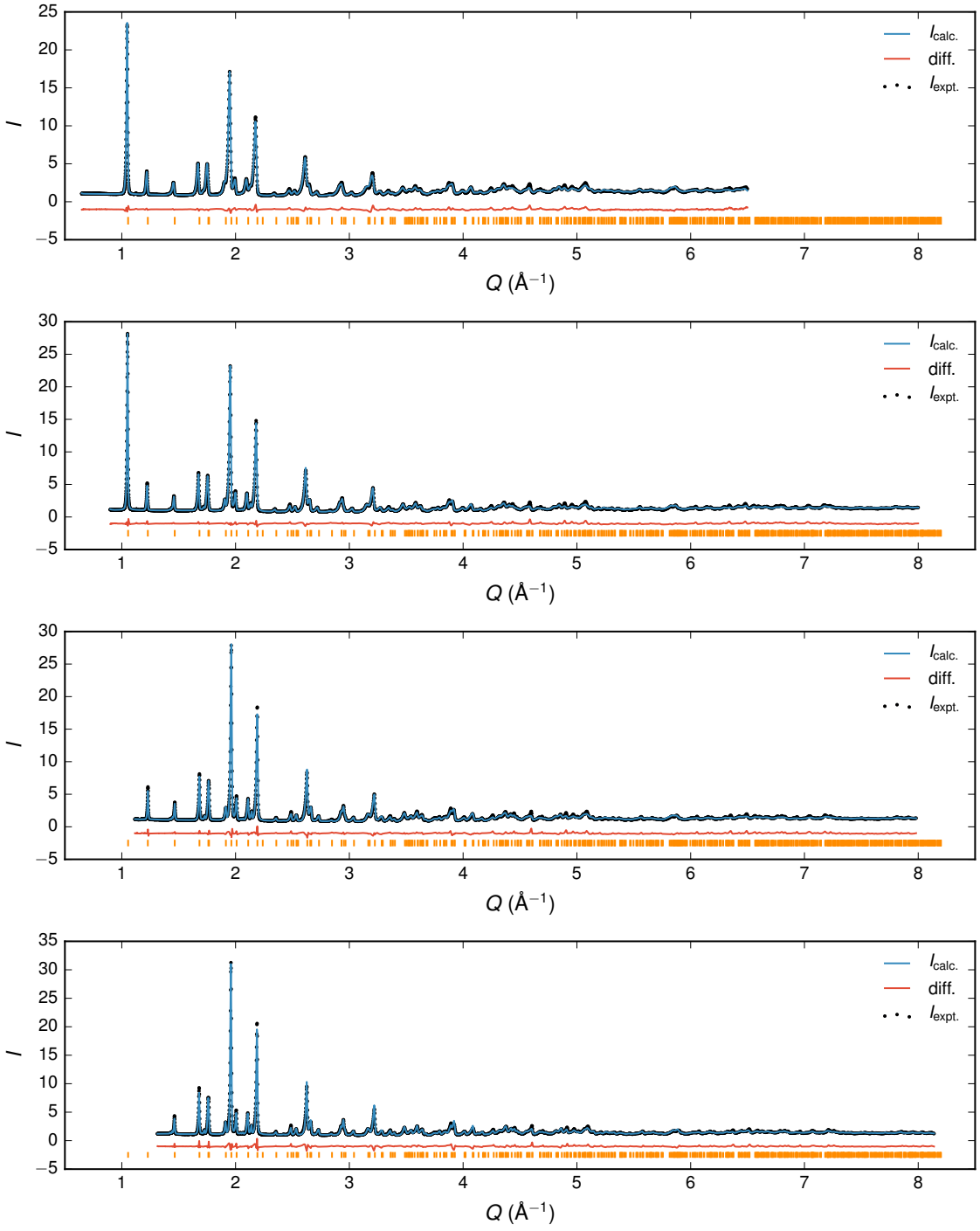

ESI Fig. 14: Neutron Rietveld Refinement at 300 K. From top to bottom, banks 2, 3, 4 and 5.

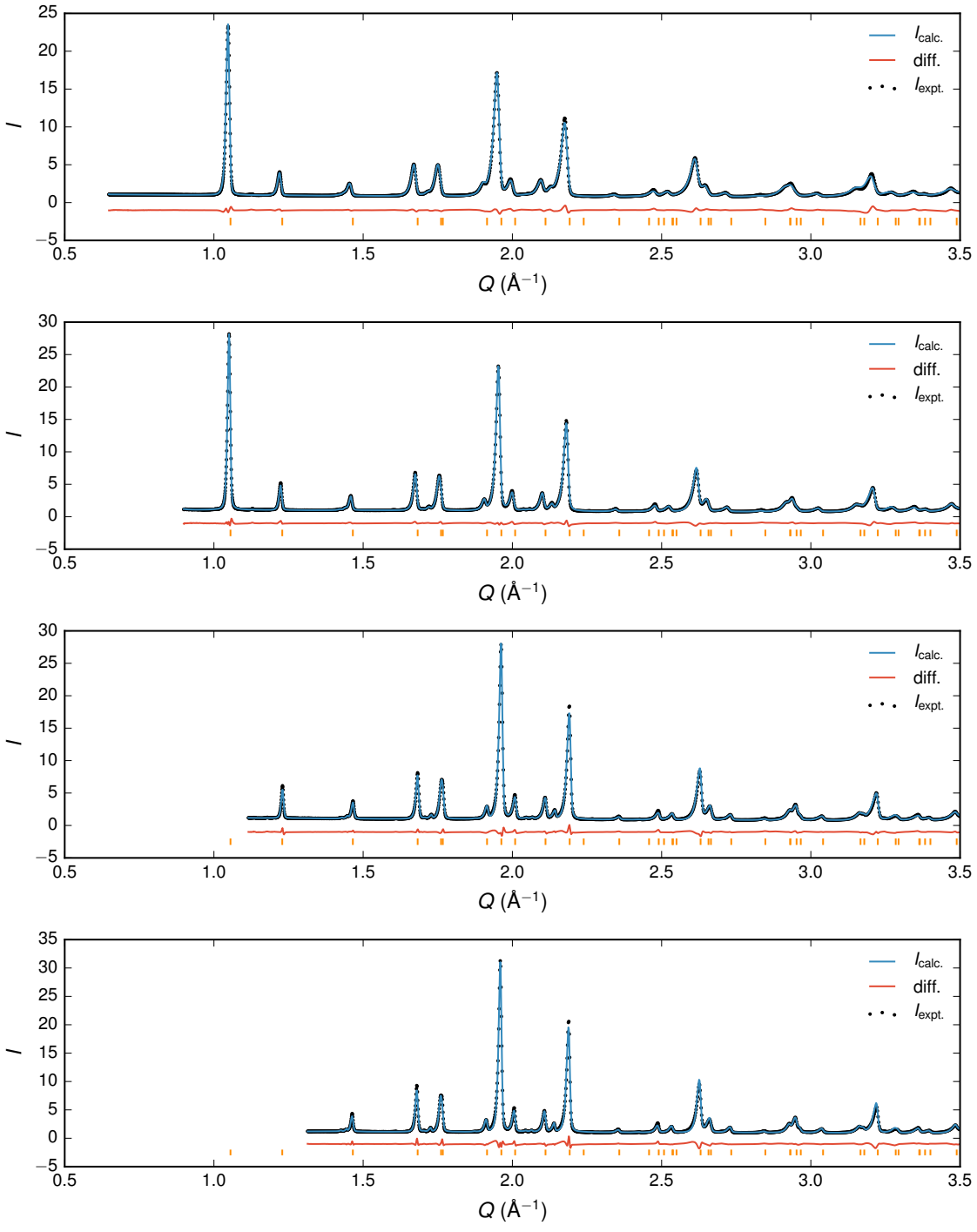

ESI Fig. 15: Neutron Rietveld Refinement at 300 K for the low Q region. From top to bottom, banks 2, 3, 4 and 5.

ESI Table 3: Refined lattice parameters for $Cu(NCS)_2$ measured at different sources

Source	T (K)	a (Å)	b (Å)	c (Å)	$\alpha\,(^\circ)$	$\beta\,(^\circ)$	$\gamma\,(^\circ)$
Lab X-ray	12	3.8738	5.6445	6.0213	81.4204	85.5750	112.9520
	20	3.8736	5.6449	6.0215	81.4099	85.5810	112.9440
	30	3.8730	5.6446	6.0210	81.3936	85.5863	112.9290
	40	3.8738	5.6449	6.0219	81.4136	85.5783	112.9450
	50	3.8753	5.6456	6.0233	81.4416	85.5665	112.9690
	60	3.8761	5.6457	6.0239	81.4601	85.5579	112.9840
	100	3.8803	5.6472	6.0283	81.5527	85.5135	113.0510
	150	3.8885	5.6498	6.0371	81.7353	85.4206	113.1610
	200	3.8978	5.6525	6.0474	81.9410	85.3112	113.2730
Neutron	1.4	3.875671	5.654245	6.027523	81.32578	85.59079	112.826
	20	3.875771	5.651786	6.026155	81.35534	85.5937	112.8382
	80	3.884608	5.655837	6.032924	81.54464	85.52593	113.0005
	150	3.895563	5.660695	6.04633	81.75789	85.41505	113.1558
	300	3.922125	5.669722	6.078091	82.29624	85.11118	113.4571
Synchrotron	295	3.91596	5.65637	6.0677	82.3704	85.0718	113.499

ESI Table 4: Refined atomic coordinates for $Cu(NCS)_2$

Radiation	$\lambda = 0.4145376$ Å			
Formula	$Cu(NCS)_2$			
M (g mol^{-1})	179.714			
Z	1			
R_{wp}	6.673			
Goodness of fit	1.070			
R_{Bragg}	1.182			
Crystal System	Triclinic			
Space Group	$P\overline{1}$			
a (Å)	3.91596(02)			
b (Å)	5.65637(02)			
c (Å)	6.06770(03)			
α (°)	82.37048(18)			
β (°)	85.07189(18)			
γ (°)	113.49967(16)			
V (Å^3)	120.7286(9)			
Atom	x	y	z	B_{iso} (Å^2)
Cu1	0	0	0	-
C1	$-0.26002(45)$	$-0.48453(33)$	$0.78756(28)$	$1.30(4)$
N1	$0.12878(37)$	$-0.71537(25)$	$0.15861(23)$	$1.44(3)$
S1	$-0.45039(14)$	$0.22294(9)$	$0.71543(8)$	$1.611(14)$

Cu1 ADP	(Å^2)
U_{11}	$0.02473(29)$
U_{22}	$0.01389(23)$
U_{33}	$0.03187(29)$
U_{12}	$-0.00294(19)$
U_{13}	$0.00303(22)$
U_{23}	$-0.01200(20)$

Estimated standard errors are given in parentheses.

5 Additional Characterisation

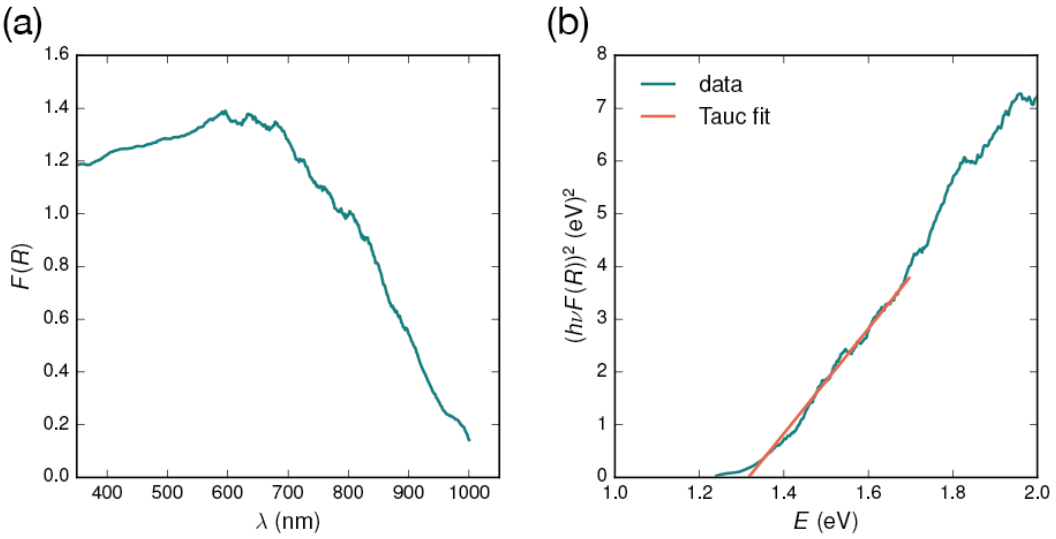

ESI Fig. 16: (a) Diffuse reflectance measured on a sample of $Cu(NCS)_2$, diluted to 10 wt% by $BaSO_4$. (b) Tauc plot for an indirect band gap, yielding a value of 1.3(1) eV.

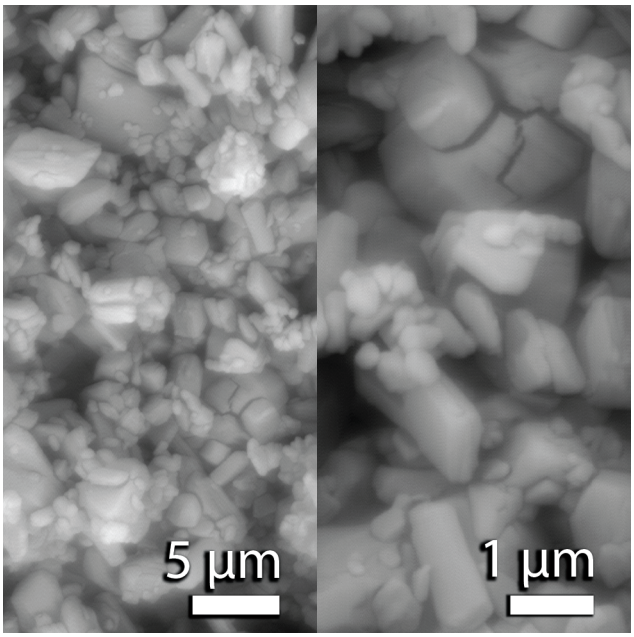

ESI Fig. 17: Backscattered electron micrographs were collected using a field emission gun scanning electron microscope (Camscan MX2600) operating at an accelerating voltage of 15 kV. 30 nm of Pt was sputter-deposited on specimens to minimize charging.

References

(S1) B. Himmetoglu, A. Floris, S. de Gironcoli, M. Cococcioni, *International Journal of Quantum Chemistry* **114**, 14 (2014).

(S2) M. Cococcioni, S. de Gironcoli, *Physical Review B* **71** (2005).

(S3) I. Bertini, C. Luchinat, G. Parigi, *Progress in Nuclear Magnetic Resonance Spectroscopy* **40**, 249 (2002).

(S4) M. Kaupp, F. H. KÃűhler, *Coordination Chemistry Reviews* **253**, 2376 (2009).